Simulating water fluxes, soil moisture and drought stress using the LWF-Brook90 hydrological model from within R.

Paul Schmidt-Walter*[a], Volodymyr Trotsiuk[b,c,d], Katrin Meusburger[b], Martina Zacios[e], and Henning Meesenburg[a]

*corresponding author (email: paul.schmidt-walter@nw-fva.de)

a: Northwest German Forest Research Institute (NW-FVA), Grätzelstraße 2, 37079 Göttingen, Germany

b: Swiss Federal Institute for Forest, Snow and Landscape Research (WSL), Zuercherstrasse 111, 8903 Birmensdorf, Switzerland

c: ETH Zürich, Department of Environmental Systems Science, Institute of Agricultural Sciences, 8092 Zurich, Switzerland

d: Faculty of Forestry and Wood Sciences, Czech University of Life Sciences Prague, Kamycka 129, Prague, Czech Republic

e: Bavarian State Institute of Forestry (LWF), Hans-Carl-von-Carlowitz-Platz 1, 85354 Freising, Germany

This document is the accepted manuscript version of the following article: Schmidt-Walter, P., Trotsiuk, V., Meusburger, K., Zacios, M., & Meesenburg, H. (2020). Advancing simulations of water fluxes, soil moisture and drought stress by using the LWF-Brook90 hydrological model in R. Agricultural and Forest Meteorology, 291, 108023 (13 pp.). https://doi.org/10.1016/j.agrformet.2020.108023

Keywords

climate impact; model calibration; water balance; forest transpiration, evapotranspiration; short rotation

Highlights

- Sensitivity analysis of LWF-Brook90 revealed a distinct parameter importance ranking
- Bayesian calibration indicated high water use for a poplar short rotation forest
- The LWF-Brook90 SVAT model excellently captures temporal variations of soil moisture
- The LWFBrook90R package facilitates complex statistical analysis and parallelization
- The modelling case study with code examples demonstrates the utility of the R package

Abstract

Soil vegetation atmosphere transport (SVAT) models are important for the quantification of water fluxes, soil water availability, drought stress and their uncertainties under climate change. We present `LWFBrook90R`, an enhanced implementation of the well-established, process-based SVAT model LWF-Brook90 for the R environment for statistical computing. The package provides new functions and sub-models for model parameterization, and facilitates parallel computing, sensitivity analysis and inverse calibration of the model. The potential of the package is demonstrated by a case study comprising i) basic forward water balance simulations for temperate grassland vegetation, deciduous and evergreen forest, ii) a parallelized sensitivity analysis, and iii) Bayesian calibrations based on soil water storage observed in a poplar (*Populus nigra* × *P. maximowiczii*) Short Rotation Forest (SRF). The sensitivity analysis revealed parameters affecting plant-available soil water storage capacity and the vegetation's timing and level of water demand to be most important for the annual course of simulated soil water storage, with seasonal and interannual differences in parameter importance rankings. The subsequent calibration yielded a very high agreement between daily simulated and observed soil water storage (0-200 cm soil depth) for the calibration and validation datasets, with Nash-Sutcliffe efficiencies of 0.97 and 0.95, respectively. The final model predicted high though realistic rates of annual evapotranspiration (2011: 844 ± 3.8 mm y^{-1}, 2012: 733 ± 4.5 mm y^{-1}) for the poplar SRF, regularly exceeding grass reference evaporation (ET_0) by 20-47% during the months of the growing season. However, basing calibrations solely on observed soil water storage probably resulted in biased partitioning of evapotranspiration towards interception losses. The integration of the LWF-Brook90 hydrological model into R with its wide variety of extensions was successfully tested and may provide efficient, reliable and reproducible water balance predictions by facilitating complex statistical analyses and large-scale applications of the model.

Software availability

The `LWFBrook90R` source code is publicly available at https://github.com/pschmidtwalter/LWFBrook90R and runs with R >= 3.1.0. The package imports functionality from R-packages `data.table`, `vegperiod`, `sirad`, `foreach`, `doSNOW` and `snow`, which can be installed from *The Comprehensive R Archive Network* (CRAN).

1 Introduction

Water availability plays a key role in the productivity and vitality of terrestrial ecosystems and is becoming increasingly important against the background of climate change. For forests, substantial impacts of water shortage have been reported (Allen et al., 2015), including large-scale die-back, productivity declines and increased vulnerability to insect infestations after cumulative and extreme drought events (Seidl et al., 2007). Due to the ongoing and predicted alterations of precipitation patterns and increasing evaporative demand caused by rising temperatures, the severity of droughts is expected to increase in many parts of the world, with unprecedented effects on forest structure and composition concerning even ecosystems to date not being considered water-limited (Allen et al., 2010). Anticipating future water availability patterns and growth conditions of forests, therefore, is crucial, and a prerequisite for developing and implementing mitigation and adaptation strategies (Lindner et al., 2010).

Soil water dynamics, drought stress and the water balance of forest ecosystems are characterized by complex interactions between climate, soil and vegetation. Process-based soil vegetation atmosphere transport (SVAT) models can capture temporal soil moisture dynamics, and therefore are key tools for understanding and predicting water fluxes, soil water availability and drought stress of forest stands (Arora, 2002; Bouten and Jansson, 1995; Federer et al., 2003; Speich et al., 2020; van der Salm et al., 2007). At the national to regional scale, SVAT models have been connected to climate projections, soil grids and forest inventory data, to determine recent and future trends of water availability and drought stress in climate impact assessment studies (De Cáceres et al., 2015; Ruffault et al., 2014, 2013; Schmidt-Walter et al., 2019; Schwärzel et al., 2009; Thiele et al., 2017), providing information on future ecosystem services, forest growth conditions, and species suitability to design and implement mitigation and adaptation strategies (Lindner et al., 2010). At the local scale, SVAT models are applied to derive drought indicators (for an overview see Speich, 2019) to understand vitality patterns and growth depressions of forests (Granier et al., 2007; Lebourgeois et al., 2005; Manrique-Alba et al., 2017; Michelot et al., 2012), tree mortality (Allen et al., 2010; Seidl et al., 2017), to estimate crop water requirements (Fischer et al., 2018), and to explain secondary drought-related impacts on forests, such as insect infestations (Netherer et al., 2019). Apart from such explanatory applications, SVAT models also offer estimates of water balance components that are

difficult to obtain from field measurements (e.g. seepage flux), and allow for partitioning evapotranspiration into transpiration, interception and ground evaporation (van der Salm et al., 2007).

Despite their widespread use, the complexity of simulated processes challenges the routine application of SVAT models. Numerous parameters have to be defined, many of which cannot be obtained from field observations directly (Franks et al., 1997). To improve the models' capacity in reproducing field observations of, e.g. soil moisture or evapotranspiration, parameter adjustments are often required. In this process, sensitivity analysis and model calibration are important tasks, allowing for an efficient estimation of model parameters and their uncertainties referenced by observations (Song et al., 2015). Sensitivity analyses evaluate the effects of the model input on model output variability (Pianosi et al., 2016), thereby providing insights into model behavior under changing model parameters, and helping to identify influential parameters to adjust in calibration. For calibration, Bayesian data integration or inverse modelling has been recommended as the most powerful technique for parameter estimation (Hartig et al., 2012; van Oijen, 2017). Compared to other calibration techniques, these methods offer a proper statistical framework for quantifying uncertainties in model parameters and model predictions. Aside from their bare scientific value, the quantification of uncertainties in model predictions (e.g. as confidence bounds of model forecasts) is also increasingly demanded by decision-makers. Bayesian data integration techniques therefore have recently become increasingly popular (Post et al., 2017; Raj et al., 2018), helping to derive reliable and robust parameter sets. Reliable parameter sets, in turn, are key prerequisites for larger scale forward simulations aimed at predicting the bounds of system behavior in a future climate, beyond observations.

The integration of complex statistical analyses, such as sensitivity analysis and Bayesian data integration, into SVAT models and other numerical models, however, is tedious. For performance reasons, the models are mostly written in compilable programming languages such as C/C++ or Fortran, requiring extensive programming skills and time resources to implement extensions that practitioners often lack. Furthermore, the models are often designed as stand-alone computer programs requiring special input data formats, which complicates the integration of driving data for executing, and observational data for calibrating and validating the model. State-of-the-art sensitivity analysis and model inversion techniques, however, are readily available in the *R Language and Environment for Statistical Computing* (R Core Team, 2019) via dedicated extension packages (e.g. (Hartig et al., 2019; Pujol et al., 2016). Moreover, *R* offers various extensions ("R packages") that are particularly useful for process-based SVAT and hydrological models (Slater et al., 2019). For instance, R packages provide for parallel processing of tasks on desktop computers and High-Performance Computation (HPC) clusters, interpolating and downscaling climate projection data (De Cáceres et al., 2018; Hanel et al., 2017; Iturbide et al., 2019), database connection interfaces (Conway et al., 2017) and advanced interactive graphics, that all help to tap data streams, speed up model execution, and analyze and

present simulation results without switching between applications. Interfacing process-based models with *R*, therefore, is highly advantageous and has recently been put into practice for several models (Bagnara et al., 2019; Coron et al., 2017; Pullens et al., 2017; Wu and Liu, 2012).

In this study, we introduce `LWFBrook90R` (Quelle: ZENODO), a newly developed R package that makes the vast resources of the *R Environment* readily available to the widely used hydrological SVAT model LWF-Brook90 (Hammel and Kennel, 2001). The model, a well-established modification of the Brook90 model (Federer 2002; Federer et al. 2003), simulates daily transpiration, interception, soil and snow evaporation, streamflow and soil water fluxes through a soil profile covered with vegetation. The package serves as a flexible and easy-to-use interface between LWF-Brook90 and R, providing easy access to plot-level water balance simulations, and facilitating complex statistical analyses as well as large-scale applications, both supported by parallelization of the model. In the context of a case study, we here use `LWFBrook90R` to (1) study the importance model parameters for model output using sensitivity analyses, and to (2) determine parameter values and their uncertainties using Bayesian data integration, to investigate the water balance of a poplar short rotation forest (SRF). The presented methods and results provide detailed information on the use of the model and its sensitivity to input parameters, as well as original data on SRF evapotranspiration.

2 The LWFBrook90R package

With the `LWFBrook90R package`, the LWF-Brook90 hydrological model can be run directly from within R. A set of functions (Table 1) facilitates simulation, set up and model execution with only few commands. The package core function `runLWFB90` constructs the model input objects from model control options, parameters, climate and soil data, and executes LWF-Brook90. After the simulation has terminated, user-selected results are returned together with the model input.

Table 1: Main functions of the `LWFBrook90R` package.

Name	Category	Description
runLWFB90()	*model execution*	Runs the LWF-Brook90 hydrological model using model control options, parameters and meteorology data input objects
mrunLWFB90()		Performs a multi-run simulation using a set of variable input parameters
msiterunLWFB90()		Performs a multi-site run using lists of climate, model control options, and parameter input objects
r_lwfbrook90()		Low-level interface function to the LWF-Brook90 dynamic library
setoptions_LWFB90()	*model set up*	Creates a model control options object
setparam_LWFB90()		Creates a model input parameter object

The model control options thereby contain information about the type of radiation input (global radiation or sunshine duration), the temporal resolution of precipitation input (and the simulation time-step), the use of precipitation correction functions, and the type of water retention and unsaturated hydraulic conductivity model (Table 2). Aside from these basic simulation settings, the user can select from several sub-models for defining aboveground stand properties, leaf area index (LAI) dynamics, phenology, and root length density depth distributions (Table 2). All methods and sub-models previously available in an MS Access user interface for the LWF-Brook90 model have been included and are continuously extended by additional sub-models. Furthermore, ancillary functions help to set up the options and parameter input objects conveniently and to estimate soil hydraulic properties from soil physical data using pedotransfer functions. To preserve the execution speed and to warrant platform-independent usability of the model, the LWF-Brook90 Fortran code was embedded directly into the package as a dynamic library, which is compiled upon package installation. Compiling from source files makes the `LWFBrook90R` package fully operational on Windows, MacOS and Linux operating systems.

Table 2: Methods and sub-models currently available in the `LWFBrook90R` model control options.

Name	Description	Options
fornetrad	type of radiation input data	'globrad' (global solar radiation) or 'sunhours' (sunshine duration hours)
imodel	type of water retention and unsaturated hydraulic conductivity model	'CH' (Clapp and Hornberger, 1978) or 'MvG' (Mualem, 1976; van Genuchten, 1980)
prec.interval	number of precipitation input intervals per day and simulation time step	1 (daily values) to 240 (6 minutes intervals)
prec.corr	correction of precipitation input for evaporation and wind loss	'yes' (Richter, 1995) or 'no'
budburst.method	air temperature based phenology models to calculate the dates of budburst (all methods available in R-package 'vegperiod' (Nuske, 2017))	'Menzel' (Menzel, 1997, 10 tree species), 'ETCCDI' (Frich et al., 2002), 'Ribes uva-crispa' (Janssen, 2009), 'fixed' (no model, dates specified in parameters)
leaffall.method	air temperature based phenology models to calculate the beginning of leaf fall (all methods available through R-package 'vegperiod'; Nuske, 2017)	'vonWilpert' (von Wilpert, 1990), 'LWF-BROOK90' (Hammel and Kennel, 2001), 'NuskeAlbert', 'ETCCDI' (Frich et al., 2002), 'fixed' (no model, dates specified in parameters)
lai.method	method name for constructing the seasonal course leaf area index development from parameters	'b90' (Hammel and Kennel, 2001), 'linear' (interpolation), 'Coupmodel' (Jansson and Karlberg, 2004)
standprop.input	type of input for annual plant characteristics (max. LAI, SAI, stand height, stand density)	'parameters' or 'table'
standprop.interp	interpolation method for constructing daily plant characteristics (except for LAI) from annual values	'constant' or 'linear' (changing) during the year
standprop.use_ growthperiod	Shall intraannual changes in plant characteristics (except for LAI) and age-dependent root growth exclusively take place between the dates of budburst and beginning of leaffall?	TRUE or FALSE
root.method	method name for constructing the root length density depth distribution	'betamodel' (Gale and Grigal, 1987), 'table', 'constant', 'linear' (depth interpolation)

The model can be used for single run simulations, where the water balance of a single site is simulated using a predefined set of input parameters (Table 1). A basic application would be to run a simulation, inspect the results, adjust selected parameters, and rerun the simulation. This highly interactive workflow is supported by the properties of R as an interpreted language and makes it very easy for new users to get familiar with the results and the influence of single parameters in LWF-Brook90. Such single run simulations can be extended by:

1. Variation of model input parameters in sensitivity analyses and model calibration tasks,
2. Forward simulations for multiple locations, parameter sets, or climate scenarios.

For the first task, the function `mrunLWFB90` (Table 1) can be used as a flexible tool to perform multiple simulations that incorporate a given variation of selected input parameters in Monte Carlo simulations. For the second task, the function `msiterunLWFB90` can be used, running the model on multiple sites using individual parameter sets, soil and climate data inputs. Both functions support parallel processing of the individual model runs for personal computers, computational servers and HPC clusters. In this way, large forward simulations, as well as sensitivity analysis techniques using Monte-Carlo simulations (Saltelli et al., 2008) or informal inverse calibrations such as the Generalized Likelihood Uncertainty Estimation (GLUE) procedure (Beven and Binley, 1992), that both require thousands of model runs (Bagnara et al., 2019) can be carried out efficiently.

Formal Bayesian calibrations can be performed by connecting `LWFBrook90R` to one of the various R packages offering inverse modelling. The connection can be set up by specifying a likelihood function that links a set of model input parameters to a likelihood measure for producing an observed output, by evaluating the differences between model predictions and independent observations. All functions for generating model input from parameters and model control options, the low-level interface function to the dynamic library itself (Table 1), and a set of functions for processing model output are available to the user. As such, `LWFBrook90R` can serve as a toolbox for flexibly specifying custom likelihood functions. Such a likelihood function can then be sampled by one of the various algorithms available in, e.g., the R package `BayesianTools` (Hartig et al., 2019).

3 Case study

We present a case study in which we investigate the water balance of a poplar (*Populus maximowiczii* × *P. nigra*) SRF using `LWFBrook90R`. For this purpose, we first conduct a sensitivity analysis to identify important model parameters. Subsequently, we perform Bayesian model calibrations using observations of daily bulk soil water storage. Finally, a forward simulation is done using the joint posterior parameter distribution, in order to derive estimates of the plantation's water fluxes and their uncertainties. To compare the estimated water fluxes to other vegetation types, a set of single run

simulations is initially performed. The R code and detailed instructions for each task are provided along with package installation information (Appendix A) and the required data sets in the supplementary material to the paper.

3.1 Study site and data acquisition

The study site is located on a deep loess soil over gravel deposits near Kaufering (600 m a.s.l.), S-Germany (48°05'13''N, 10°51'39''E), on former crop land. Mean annual temperature is 8.4°C (1981-2010), mean annual precipitation is 996 mm, with a maximum in the summer months typical for the pre-alpine landscape in which the study site is located. The SRF was planted in 2008 from cuttings, had an average tree height of 9 m in 2011 and a closed canopy with a maximum LAI of ca. 6 m^2 m^{-2}. Meteorological data were obtained from the German Weather Service's nearby station in Landsberg. In a soil inventory, soil physical properties were determined, from which the soil hydraulic parameters were estimated using pedotransfer functions (Puhlmann and von Wilpert, 2012). In 2011 and 2012, volumetric soil water content was measured in 15, 50, 115, 160 and 220 cm soil depth using FDR probes (10HS, Decagon Devices, Inc.). The measurements were interpolated and integrated across the soil profile to obtain daily bulk soil water storage in 0-200 cm soil depth, which is the basis for calibrating and validating the model.

3.2 Single run simulations

3.2.1 Simulation set up

Three single run simulations were performed to provide references for the SRF water balance estimated in section 3.4.2, and to demonstrate the basic use of the package (Appendix B). The three simulations represent a temperate deciduous beech forest stand, a temperate evergreen spruce forest stand and a temperate grassland vegetation cover. The characteristic parameters of the vegetation types (Table 3) were obtained from Federer et al. (1996), with modified interception parameters for the forest cover types from Schmidt-Walter et al. (2019). The simulations were run for the period 1980-2010, and made use of the option to estimate the dates of budburst, i.e. when LAI starts to increase, following the degree-day approaches described in Menzel (1997; deciduous, evergreen) and Frich et al. (2002; grass). Along with other approaches (Table 2), these are available in `LWFBrook90R` by importing the R package `vegperiod` (Nuske, 2017). The end of the growing season, when LAI starts to decline, was estimated using the methods described by von Wilpert (1991) for the forest cover types, and again Frich et al (2002) for the grassland vegetation. The root density depth distributions of the vegetation types were generated using the β model (Gale and Grigal, 1987), with coefficients taken from Jackson et al. (1996).

Table 3: Input parameters sets for the three vegetation cover types. All other model parameters are set to default values.

Parameter	Description	Unit	Temp. evergreen forest	Temp. deciduous forest	Temp. grassland
maxlai	Max. LAI in summer	$m^2\ m^{-2}$	6	6	3
winlaifrac	Min. LAI in winter as fraction of maxlai	-	0.8	0	0.5
height	vegetation height	m	25	25	0.5
sai	stem area index	$m^2\ m^{-2}$	0.875	0.875	0
glmax	maximum leaf conductance	$m\ s^{-1}$	0.0053	0.0053	0.0053
radex	radiation extinction coefficient	-	0.5	0.6	0.7
alb	albedo	-	0.14	0.18	0.2
albsn	albedo ground covered with snow	-	0.14	0.23	0.5
maxrlen	max. fine root length	$m\ m^{-2}$	3100	3500	1000
betaroot	beta coefficient root distribution	-	0.976	0.966	0.943
maxrootdepth	max. root depth	m	-1.2	-1.4	-0.8
lwidth	average leaf width	m	0.004	0.05	0.006
frintlai	interception catch fraction of rain per unit LAI	-	0.12	0.12	0.06
frintsai	interception catch fraction of rain per unit SAI	-	0.14	0.25	0.06
cintrl	interception storage capacity for rain per unit LAI	$mm\ m^{-2}$	0.2	0.2	0.15
cintrs	interception storage capacity for rain per unit SAI	$mm\ m^{-2}$	0.4	0.4	0.15

3.2.2 Results and discussion

The simulated annual course of water fluxes shows a maximum of evapotranspiration E (i.e., the sum of actual transpiration T_a, interception E_i, and soil evaporation E_s) in the summer months, and a maximum of total runoff (i.e., sum of drainage water flux D, and surface runoff R) in late winter or early spring (Figure 1). The highest mean evapotranspiration rates (1981 to 2010) thereby originate from the evergreen spruce forest (864 mm y^{-1}), followed by the deciduous beech forest (685 mm y^{-1}) and the grassland vegetation (593 mm y^{-1}). Accordingly, average total runoff from the soil profile (beech 307 mm y^{-1}; spruce: 137 mm y^{-1}; grassland 402 mm y^{-1}) is highest under grassland and lowest under spruce, and is predominantly routed to groundwater as drainage flux (D) from the bottom of the

soil profile. The simulation results and mean water fluxes generally agree with observations for these vegetation types in the pre-alpine landscape (beech: Baumgarten et al., 2014; grassland: Fu et al., 2017; spruce, beech: Weis et al., 2012).

For all vegetation types, the main evapotranspiration component is T_a, and more or less pronounced transpiration deficits (T_D) develop in late summer (Figure 1). As a measure drought stress, the transpiration deficit quantifies the difference between potential and actual transpiration, with the latter being reduced below potential transpiration LWF-Brook90, when water uptake is limited due to low soil water availability. Among vegetation types, distinct differences in the annual courses of evapotranspiration fluxes can be observed. Due to the permanent foliation of the evergreen spruce forest and grassland, small amounts of transpiration also occur in winter, and water uptake starts earlier in the year compared to the deciduous forest. In deciduous forest, soil evaporation (E_s) is the main component of evapotranspiration in early spring. Even greater differences can be observed for the annual courses of interception evaporation (E_i). While E_i in the dormant season is low for the deciduous and grassland vegetation, the evergreen spruce forest shows comparably high amounts of interception evaporation throughout the year.

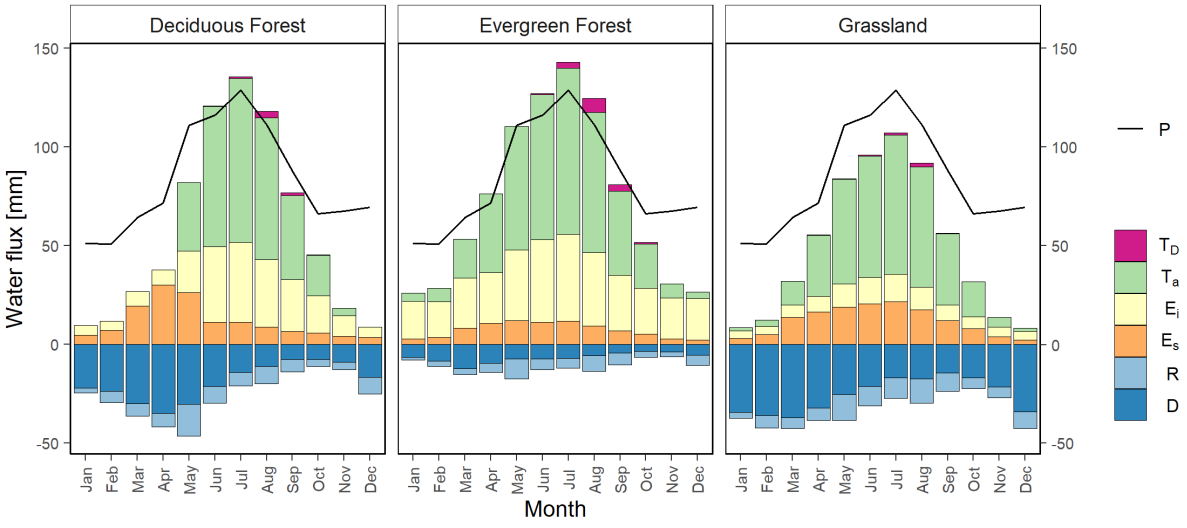

Figure 1: Mean monthly precipitation (P), actual transpiration (T_a), rain and snow interception evaporation (E_i), soil and snow evaporation (E_s), drainage (D, displayed as negative values), surface runoff (R, displayed as negative values), and transpiration deficit (T_D) of the three cover types for the period 1981 to 2010. T_D greater zero refers to a reduction of T_a below potential transpiration, indicating drought stress.

Other model outputs of plant physiological interest are the soil matrix potential (Figure 2 a) and the relative extractable soil water storage (REW, Figure 2 b). REW is a measure of relative water availability in the root zone, and is calculated as the ratio between actual plant available soil water (difference between actual water content and water content at wilting point, Ψ=1600 kPa) and plant available water capacity (water content difference between field capacity, Ψ= 6.3 kPa, and wilting point). Soil water availability is considered to severely limit transpiration of forest ecosystems, when REW falls below 0.4 (Granier et al., 2000).

During the growing season, evapotranspiration exceeds precipitation, causing a decrease in soil moisture, as expressed by a decline of Ψ and REW (Figure 2). Under forest cover, the reduction of Ψ extends to greater soil depths as compared to the grassland cover, due to a deeper rooting system of the trees (Figure 2 a). At minimum values below -225 kPa, the evergreen spruce forest on average shows the most intensive and profound reduction in matrix potential, also affecting soil layers below the root zone. This is also reflected in the highest mean transpiration deficit (T_D, Figure 1) and the lowest median values of REW (Figure 2 b), compared to the other vegetation types. While in the deciduous forest and grassland vegetation, the critical threshold at REW = 0.4 is undercut only by the absolute minimum REW values, even the 10%-quantile falls below the critical limit under evergreen forest, indicating that limited water availability in summer is more the rule than the exception in the spruce forest.

At the end of the growing season, soil water replenishment sets in, recovering Ψ. For the grassland, high values above -5 kPa that indicate field capacity is quickly approached after water uptake ceases in autumn. Under deciduous beech, soil water replenishment is completed around the turn of years. In contrast, the replenishment of the subsoil at the evergreen spruce forest on average remains incomplete until the onset of the growing season. This indicates that for spruce, the large soil water deficits from the growing season, and a higher interception evaporation in the dormant season do not allow for a thorough soil rewetting in every year of the simulation. In fact, the 10%-quantile of REW stays below 1 (Figure 2 b), suggesting that in some years, the root zone water storage is not refilled completely under spruce. In this way, soil water deficits can build up across years, making this vegetation type particularly vulnerable to cumulative-type droughts. In contrast, the highest values of even the minimum REW exceed 1 in the other vegetation types, revealing a complete refill of the root zone soil water storage under deciduous forest and grassland vegetation in every year’s winter or early spring.

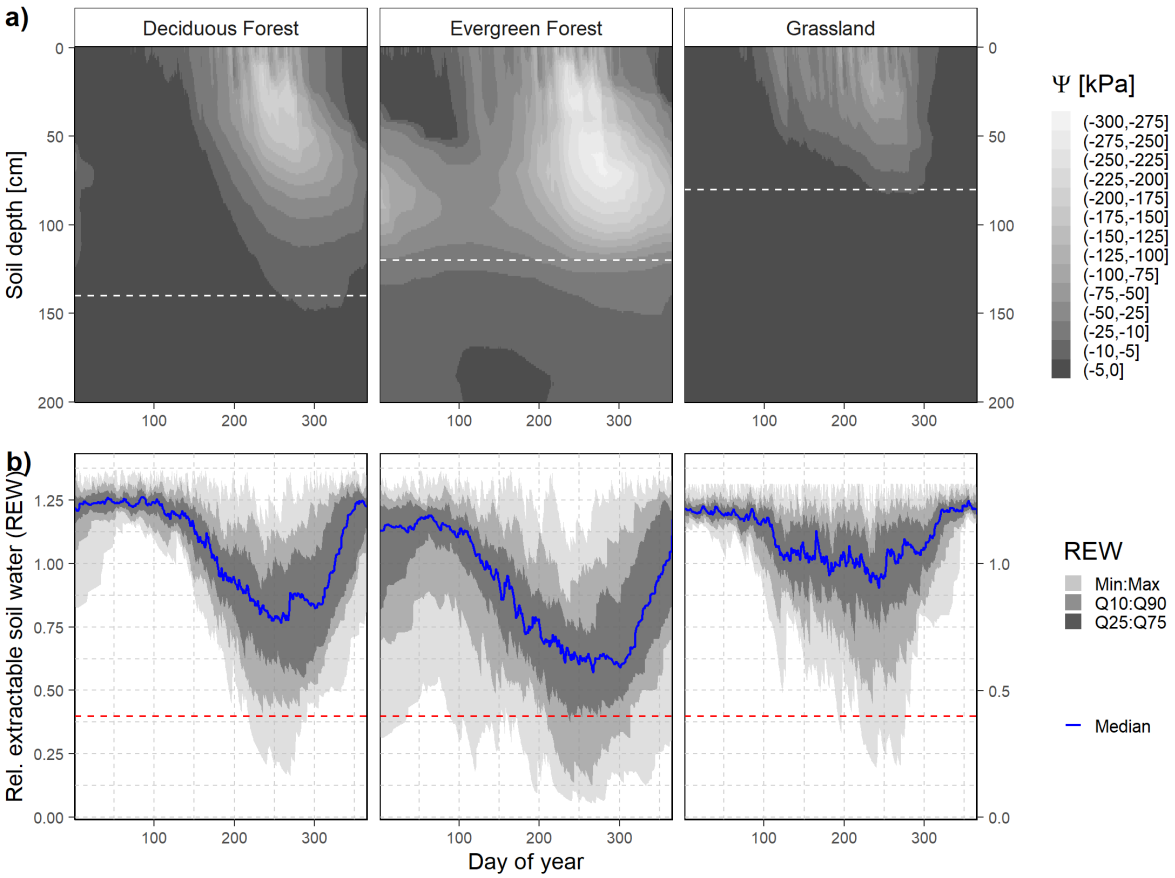

Figure 2: a) Depth-interpolated mean daily soil water potential (Ψ), and b) distribution statistics of relative extractable soil water (REW) for the three vegetation types in the period 1981-2010. Mean daily soil water potential of the soil layers was depth-interpolated and classified to discrete values. The dashed lines refer to the root depths of the vegetation types (a), and the critical threshold value (b) at REW = 0.4 (Granier et al., 2000).

3.3 Sensitivity analysis

Before calibrating LWF-Brook90 to soil water storage observed at the poplar plantation, we conducted a regional sensitivity analysis (Hornberger and Spear, 1981; Saltelli et al., 2008) to identify parameters that have a positive effect on the agreement between simulated and observed soil water storage. In regional sensitivity analyses (also called "Monte Carlo Filtering"), a large parameter sample is evaluated in a Monte-Carlo simulation and subsequently split into 'behavioral' and 'non-behavioral' subsets, corresponding to model output below or above a certain threshold (Pianosi et al., 2016). To measure the agreement between simulated and observed bulk soil water storage in 0-200 cm soil depth, we calculated Nash-Sutcliffe efficiency (NSE) and considered all simulations having NSE $\geq$ 0.8 as behavioral. In order to determine the sensitivity of simulated soil water storage to the individual parameters in different years and seasons, we determined several NSE values, referring to the whole simulation (2011-2012), the two years separately (2011, 2012), the growing (April-September) and dormant seasons (October-March). The importance of individual parameters in each of the different observation periods was evaluated by testing the behavioral parameter distributions for differences to the non-behavioral parameter distributions, using the two-sample Kolmogorov-Smirnov test. The test-statistic D_{max} thereby describes the maximum distance between the empirical cumulative distribution

functions (ECDFs) of the behavioral and non-behavioral parameter sets, and serves as a measure of parameter importance for the investigated model output.

3.3.1 Simulation set up

Out of the ca. 100 LWF-Brook90 model input parameters, we analyzed 24 parameters for their impact on model performance, as referenced by observed bulk soil water storage. The parameters included variables affecting potential transpiration, water uptake and leaf water supply, interception evaporation, soil hydraulic properties and phenology. Maximum leaf area index (LAI), which is used LWF-Brook90 to upscale leaf-level parameters to the canopy, was fixed to the observed 6 m^2 m^{-2} and not set up for variation. The parameter sample (N=50,000) was generated from random uniform distributions, with variation ranges (Table 4) derived from the literature (Federer, 2002; Federer et al., 2003; Groh and Puhlmann, 2013), or set to the feasible parameter range when no information was found. For the soil porosity and saturated conductivity parameters of the single soil layers' hydraulic properties, we used scaling factors to vary the values of all soil layers simultaneously. The variation range for the layers' porosities was defined as ±25% around the initial value. The layers' saturated hydraulic conductivities were varied on a logarithmic scale of base 10 by ±0.5 magnitudes. The 50,000 simulations were run from 2010 to 2012 (2010 serving as spin-off period), using the function `mrunLWFB90` on a computation server with 10 processors in parallel. The simulations took less than 4 hours to execute, but could also have been run overnight on a desktop computer using three CPUs. The R code and detailed instructions are provided in Appendix C and additionally include visualizations of the behavioral parameter distributions (Figure C3), and simulated soil water storage compared to observations (Figure C4).

3.3.2 Results and discussion

The sensitivity analysis revealed a distinct ranking of the individual parameters' importance for achieving simulations in the behavioral model region (NSE ≥ 0.8 for soil water storage in 0-200 cm soil depth). Considering the entire simulation period (2011-2012, Figure 3), the scaling factor for the soil layers' individual porosity (*sc_ths*) was most important (classified as 'highly important', $D_{max} \geq$ 0.2, Harlin and Kung, 1992), followed by the β coefficient of the vertical root distribution (*betaroot*), the date of budburst (*budburstdoy*), and the factor reducing leaf conductance for low solar radiation (*r5*). Together with the maximum leaf conductance (*glmax*), these parameters define the vegetation's timing and level of water demand (*budburstdoy*, *glmax*, *r5*), and plant available water storage capacity of the soil profile (*sc_ths*, *betaroot*). Their importance for soil water storage, as well as the importance of the individual soil layers' saturated hydraulic conductivities (*sc_ksat*), is expressed in almost all investigated periods ($D_{max} \geq 0.1$, Table 4), at varying degrees. The influence of other parameters in some cases was significant, but their influence on model performance mostly unimportant ($D_{max} <$ 0.1), with exceptions for the growing season (April-September) concerning the interception storage

capacity *(cintrl)*, soil evaporation resistance *(rssa)* and critical leaf water potential at which stomata close (*psicr)*.

The importance of parameters differed between seasons and years. Only subsets of parameters were important for acceptable model fits of soil water storage in the dormant season (October-March) or the individual years (Table 4). In particular, the date of budburst (*budburstdoy*), *rssa*, *cintrl* and saturated hydraulic conductivities (*sc_ksat*) were unimportant ($D_{max} < 0.1$) in the dormant season, and the parameters affecting potential transpiration and leaf water supply were naturally less important for soil water storage compared to the growing season. For the two years, differences mainly concerned the ranking of parameters affecting potential transpiration (*glmax*, *r5*) and root zone water storage (*sc_ths*, *betaroot*). In contrast to 2011, potential transpiration parameters in 2012 appeared to be unimportant, while higher importance was assigned to the β coefficient of the root length density depth distribution (*betaroot*), and the scaling parameters for soil porosities and saturated hydraulic conductivities (*sc_ths*, *sc_ksat*). This indicates that the annual course of soil water storage in 2012 was more sensitive to plant-available soil water storage capacity than water demand, when compared to 2011.

The general ranking of parameters we found is in accordance with Federer et al. (2003), who indicate that apart from climatic conditions, highest impacts on annual evapotranspiration result from the vegetation cover type and the available soil water capacity. In our analysis, these two factors are represented by the parameters affecting potential transpiration, total soil water storage capacity and root distribution (Table 4). However, the ranking of input parameter importance (Figure 3) only partly agrees with the findings of the so-far single sensitivity study of LWF-Brook90 model performance referenced by observations of soil moisture (Groh and Puhlmann, 2013). Following Groh and Puhlmann (2013), we identified the soil porosity to be the most important parameter for model performance. However, the other parameters we found to be highly important (*budburstdoy*, *r5*) were not tested in the study of Groh and Puhlmann (2013), or were of a relatively lower or no importance compared to our analysis (e.g. *betaroot, glmax, mxkpl*). Other parameters that here did not affect model performance, in turn, were of great importance in the other study (such as *ilayer*), that however used depth-specific measurements of water content as reference. Such data naturally are more sensitive to parameters affecting the vertical water movement through the soil (e.g., *ilayer*) than the bulk soil water storage we used.

Different model outputs, in general, show different sensitivities to individual model inputs, which complicates a comparison of model sensitivity with the available literature. Moreover, the rankings of parameter importance for a certain model output can vary from location to location (Groh and Puhlmann, 2013), and with the period represented by the model output (Song et al., 2013). Accordingly, we identified differences in the sensitivity of actual soil water storage between the two individual years, which probably were caused by the different climatic conditions in 2011 and 2012.

This indicates that sensitivity analysis should be conducted at each individual site, for which the model is calibrated.

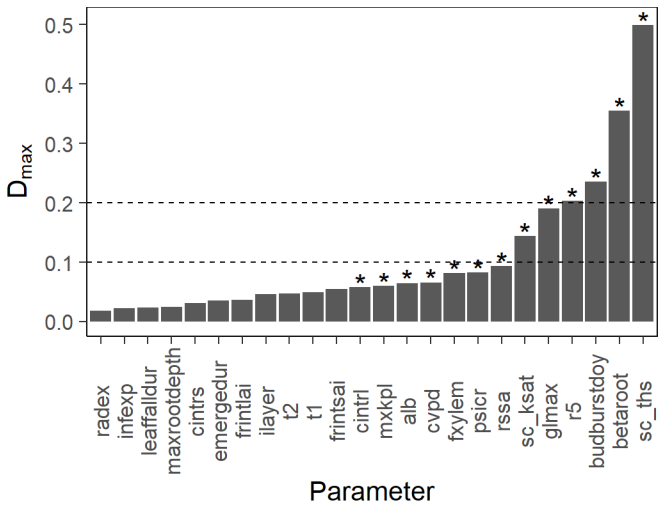

Figure 3: Maximum difference D_{max} between the ECDFs of parameter values resulting in behavioral ($NSE \geq 0.8$) and non-behavioral simulations regarding soil water storage the entire observation period (2011-2012). Reference lines are set according to the sensitivity classification after Harlin and Kung (1992): $D_{max} \geq 0.2$ = 'highly important'; $0.1 \leq D_{max} < 0.2$ = 'moderately important'; $D_{max} < 0.1$ = 'unimportant'; asterisks: significant differences between behavioral and non-behavioral parameter distributions ($p \leq 0.05$, two-sample Kolmogorov-Smirnov test).

Table 4: LWF-Brook90 parameters, their prior ranges, and importance for soil water storage measure by D_{max} in different observation periods of the simulation. Cell-shading corresponds to the sensitivity classification after Harlin and Kung (1992): dark grey = 'highly important'; medium grey = 'moderately important', light grey = 'unimportant'.

						D_{max}				
Parameter	Description	Group	Unit	Prior min	Prior max	2011-2012	2011	2012	Apr-Sep	Oct-Mar
ilayer	Macropore-assisted infiltration depth	Infiltration	-	1	13	n. sig.	n. sig.	n. sig.	n. sig.	n. sig.
infexp	Infiltration exponent	Infiltration	-	0	1	n. sig.	n. sig.	n. sig.	n. sig.	n. sig.
cintrl	Interception storage capacity for rain per unit LAI	Interception evaporation	mm m^{-2}	0.05	0.75	0.058	n. sig.	0.065	0.136	0.052
cintrs	Interception storage capacity for rain per unit SAI	Interception evaporation	mm m^{-2}	0.05	0.75	n. sig.	n. sig.	n. sig.	n. sig.	n. sig.
frintlai	Interception catch fraction of rain per unit LAI	Interception evaporation	-	0.02	0.2	n. sig.	n. sig.	n. sig.	n. sig.	0.044
frintsai	Interception catch fraction of rain per unit SAI	Interception evaporation	-	0.02	0.5	n. sig.	n. sig.	0.050	n. sig.	0.038
alb	Albedo	Energy balance	-	0.1	0.3	0.065	n. sig.	0.054	0.091	n. sig.
radex	Radiation extinction coefficient	Energy balance	-	0.4	0.7	n. sig.	n. sig.	n. sig.	n. sig.	n. sig.
budburstdoy	Day number of budburst	Phenology	day of year	90	150	0.236	0.339	0.125	0.251	0.044
emergedur	Duration of leaf unfolding	Phenology	days	5	30	n. sig.	n. sig.	n. sig.	n. sig.	n. sig.

leaffalldur	Duration of leaffall	Phenology	days	10	50	n. sig.	n. sig.	0.063	n. sig.	n. sig.
cvpd	Stomata conductance reduction factor for high vapor pressure deficit	Potential Transpiration	kPa	0.5	3	0.066	0.059	n. sig.	0.090	0.059
glmax	Maximum leaf conductance	Potential Transpiration	m s^{-1}	0.005	0.025	0.190	0.166	0.085	0.217	0.152
r5	solar radiation at which stomata conductance is half of its max. value	Potential Transpiration	W m^{-2}	50	400	0.203	0.131	0.085	0.235	0.144
t1	Air temperature below which stomata conductance is reduced	Potential Transpiration	°C	5	15	n. sig.	n. sig.	n. sig.	0.093	n. sig.
t2	Air temperature above which stomata conductance is reduced	Potential Transpiration	°C	20	35	n. sig.	n. sig.	n. sig.	n. sig.	n. sig.
rssa	Soil evaporation resistance at field capacity	Soil evaporation	s m^{-1}	20	1500	0.094	0.062	0.082	0.134	0.038
sc_ksat	Scaling factor for saturated hydraulic conductivity	Soil hydraulic properties	-	-0.5	0.5	0.144	0.054	0.130	0.190	0.055
sc_ths	Scaling factor for soil porosity	Soil hydraulic properties	-	0.75	1.25	0.499	0.489	0.501	0.460	0.495
betaroot	Vertical root distribution β-coefficient	Root distribution	-	0.9	0.999	0.355	0.125	0.260	0.381	0.257
maxrootdepth	Max. rooting depth	Root distribution	m	-2	-1.2	n. sig.	n. sig.	n. sig.	n. sig.	n. sig.
fxylem	Fraction of plant resistance in xylem	Leaf water supply	-	0.01	0.9	0.082	n. sig.	0.068	0.098	n. sig.
mxkpl	Max. hydraulic plant conductivity	Leaf water supply	mm d^{-1} MPa^{-1}	1	30	0.060	0.091	0.063	n. sig.	0.073
psicr	Critical leaf water potential at which stomates close	Leaf water supply	MPa	-4	-0.5	0.083	n. sig.	0.046	0.120	n. sig.

3.4 Bayesian calibration

Based on the results from sensitivity analysis, we set up a full Bayesian calibration, referenced by bulk soil water storage in 0-200 cm soil depth observed at the poplar SRF in Kaufering. The aim was to determine a site-specific model for quantifying the water fluxes of the plantation and their uncertainties. We set up two calibration experiments, the first using the observations from 2011, and the second using the observations from 2012 as calibration dataset, while the remaining datasets were used for validation.

3.4.1 Simulation set up

We selected the 10 LWF-Brook90 input parameters for calibration that were identified to be important for a high model performance in any of the observation periods investigated in the sensitivity analysis (Table 4). Other parameters were set to the values for deciduous forests (Table 3), except for the maximum root depth (*maxrootdepth*) and maximum LAI (*maxlai*). The former was set to a soil depth

of 2.0 m to not interfere with the β coefficient of the root distribution. The latter was fixed to the observed value of 6 m^2 m^{-2}. The simulations in both calibration experiments started one year before the actual calibration period and used the same prior parameter distributions as the sensitivity analysis.

We specified a Gaussian likelihood function to calculate the log-likelihood of a simulation given an observation and standard deviation at each calibration step. The joint posteriori parameter distribution was estimated using the Differential Evolution Markov Chain Monte-Carlo (DEzs) algorithm (ter Braak and Vrugt, 2008), implemented in the R package `BayesianTools` (Hartig et al., 2019). The total execution time for three parallel chains with three sub-chains, running in total for 300,000 iterations, was 70.5 hours.

3.4.2 Results and discussion

Posterior parameter distribution of the two calibration experiments

Both calibration experiments were successful and converged with a Gelman-Rubin point scale reduction factor close to 1. The posterior distributions were reduced over the prior parameter ranges on average by 75% (33-99%, see R in Table 5). The reduction is a measure of the width of the posterior parameter probability density distributions (Figure 4), and roughly depicts the identifiability of the parameters. In both calibration experiments, most parameters were well defined, however, the posterior distributions of *cintrl*, *r5*, and *rssa* touched the edges of their prior distributions. The soil porosity scaling factor (*sc_ths*) was defined best, with very narrow confidence bounds around 0.927 (2011) and 0.919 (2012). This corresponds to a bulk soil porosity in 0-200 cm soil depth of 712 and 705 mm respectively, which is ca. 60 mm lower than the initial soil porosity derived by the pedotransfer function. While the soil porosity was almost equal in both calibration experiments, the posterior probability density distributions of most other parameters were centered over different values. The divergence was most extreme for the soil evaporation resistance (*rssa*), which was calibrated to very high values in 2011, while very low values were found for the 2012 dataset. Clear differences in the posterior density distribution, without any overlap, were also found for the parameters *betaroot* and *budburstdoy*. For instance, low values for the β coefficient were estimated in 2012 (0.932-0.942, Tab. 5), corresponding to a more shallow root distribution with a greater proportion of roots near the soil surface (95% in 0-30 cm). This fitted distribution resembled the measured root distribution, with 88% of fine root biomass in 0-30 cm soil depth. In contrast, the root density distribution estimated for 2011 was deeper, with a less quickly depth-decreasing root density (68% in 0-30 cm).

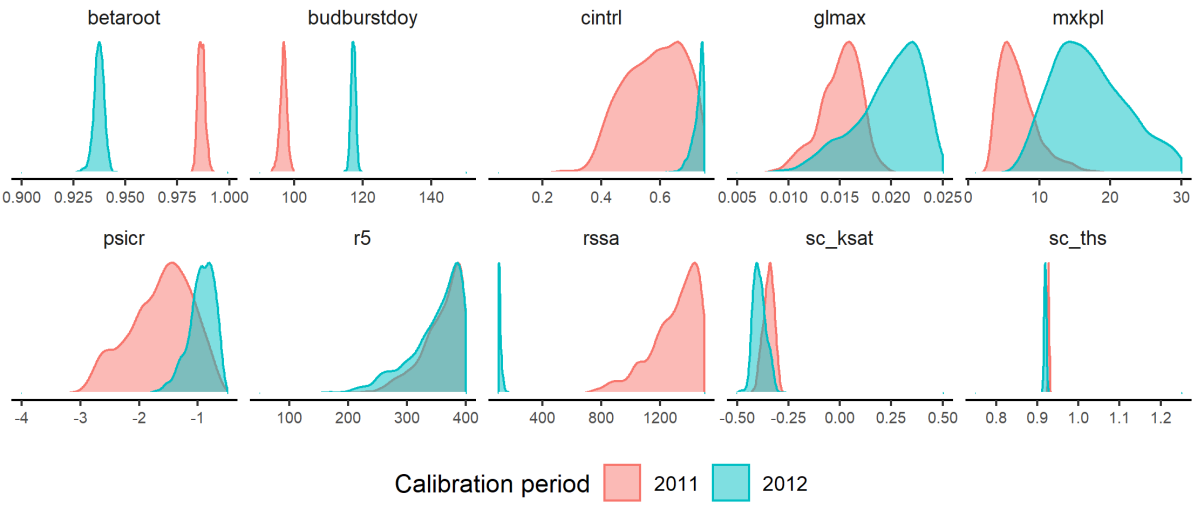

Figure 4: Posterior parameter density distributions estimated using Bayesian calibration of the LWF-Brook90 model to soil water storage (0-200 cm soil depth) observed in 2011 and 2012.

Table 5: Posterior parameter distribution statistics of the two calibration experiments. MAP is the Maximum A-Posteriori probability parameter estimate. R is reduction of posterior parameter range over prior parameter range: $R = 1 - \frac{(P_{97.5\%} - P_{2.75\%})}{(\text{prior max} - \text{prior min})}$.

		Calibration 2011					Calibration 2012				
Parameter	Unit	$P_{2.5\%}$	Median	$P_{97.5\%}$	R	MAP	$P_{2.5\%}$	Median	$P_{97.5\%}$	R	MAP
sc_ths	(-)	0.925	0.927	0.931	99%	0.926	0.914	0.919	0.924	98%	0.921
sc_ksat	(-)	-0.399	-0.343	-0.3	90%	-0.373	-0.445	-0.395	-0.326	88%	-0.376
cintrl	(mm m^{-2})	0.404	0.596	0.739	52%	0.479	0.675	0.733	0.749	89%	0.747
budburstdoy	day of year	94.502	96.774	98.747	93%	97.701	115.724	117.176	118.475	95%	117.224
glmax	(m s^{-1})	0.011	0.015	0.018	65%	0.017	0.013	0.02	0.024	45%	0.022
r5	(W m^{-2})	269.712	365.634	398.562	63%	384.354	240.585	360.399	398.041	55%	385.552
rssa	(s m^{-1})	892.05	1340.521	1493.939	57%	1428.416	100.286	107.989	141.42	97%	105.724
betaroot	()	0.984	0.987	0.99	94%	0.984	0.932	0.937	0.942	90%	0.938
mxkpl	(-)	3.592	6.807	14.443	63%	4.853	8.924	16.274	28.34	33%	16.717
psicr	(MPa)	-2.691	-1.486	-0.763	45%	-2.09	-1.458	-0.917	-0.613	76%	-0.871

Model performance

With the beginning of the growing season (April-September), observed soil water storage quickly decreased in the poplar plantation, and slowly increased in the dormant season (Figure 5). Soil water storage was above 600 mm during most of the growing season of 2011, and decreased to lower values from July 2012, indicating varying growing season water availability between the two years. In their respective calibration periods, both models provided an almost perfect fit for the timing and amount of decrease in soil water storage at the beginning of the growing seasons, but soil water storage subsequently was constantly overestimated when the wetter year was used as calibration period (Figure 5 a). This resulted in an inadequate model performance during the soil water replenishment phase at the end of the 2011, and a lower model efficiency of NSE = 0.89 (Table D1), compared to the calibration with data observed in 2012 (NSE = 0.96). The second calibration for the drier conditions in

2012 continuously provided very good results for its calibration period, with only a slight deviation between simulation and observation in autumn 2012 (Figure 5 b)

As expected, the respective validation datasets were less well represented, when compared to their respective calibration periods (Figure 5). In the first experiment (Figure 5 a), the timing of soil water storage decrease during the growing season 2012 was well reproduced, and an NSE of 0.79 was achieved for the entire validation period (2012). However, bulk soil water storage was underestimated from the beginning of August 2012, with a mean absolute error (MAE) of 18 mm. In the second calibration experiment (Figure 5 b), the model fit for the validation period (2011) was better, and in terms of model efficiency and mean absolute soil water storage error in 2011 (NSE = 0.91; MAE = 12 mm, Table D1) comparable to the values achieved in the first experiment, which used those observations as calibration dataset. Nonetheless, simulated soil water depletion at the beginning of the growing season 2011 was less strong when compared to observations. This subsequently led to slightly overestimated soil water storage in the first half of the growing season 2011, which was probably caused by assigning the inadequate estimate of the budburst-date from the year 2012 to the year 2011, where water uptake actually started to increase almost 3 weeks earlier (Figure 4).

In general, biased residuals during model validation indicate under-represented observations in the calibration dataset. In our case, the observed soil water storage during the growing season 2011 did not cover the lower values observed during the growing season 2012. From the perspective of the 2011 calibration the values observed in 2012, therefore, were located in the extrapolation region, which might explain why the course of observed soil water storage in 2012 could not be represented satisfactorily. The higher level of water availability in 2011, on the other hand, could be well represented by the 2012 calibration, which was calibrated in the year with the higher amplitude of observed soil water storage. From our experience, such effects are often observed when calibrating SVAT-models: Better results in validation are obtained when the calibration dataset includes dry years, as these hold information of how the vegetation reacts to decreased soil water availability. In contrast, wetter years often are instantly well reproduced.

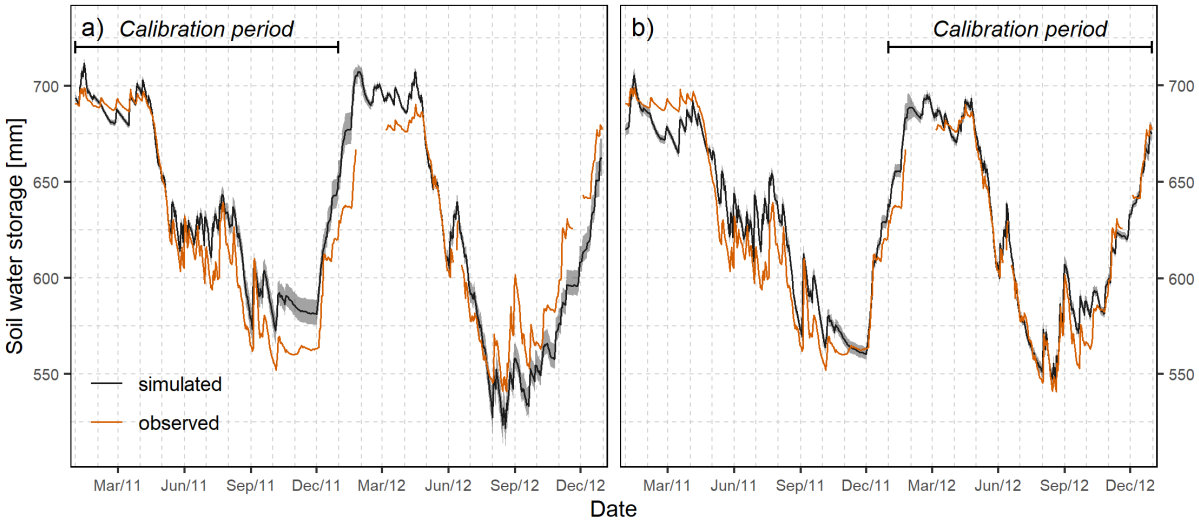

Figure 5: Comparison of observed and daily mean simulated soil water storage in 0-200 cm soil depth (n = 1000, uncertainty bounds: 95% confidence interval) for the two calibration experiments, using observations from 2011 (a) and 2012 (b) as calibration datasets.

Posterior prediction

To estimate the water fluxes of the poplar SRF, a sample (n=1000) was drawn from the joint posterior parameter distribution of the second calibration experiment. We accounted for interannual variability in the dates of budburst by independently determining the important *budburstdoy* parameter with the Menzel-model (1997), instead of using the estimated value from the calibration. We applied the Menzel-parameters for downy birch (*Betula pubescens*, Ehrh.), which produced budburst-dates close to the ones estimated in the calibration experiments. This set-up improved the model efficiency in the validation period 2011 (NSE = 0.95, Table D2), and the model performed equally well in the calibration and validation periods, the resulting model outputs therefore can be considered as reliable estimates of evapotranspiration and runoff for the poplar SRF in Kaufering. To compare the estimated water fluxes of the plantation to other vegetation types, the simulations from section 3.2 were rerun, now using the estimated scaling factors for soil porosity and saturated hydraulic conductivity (Table 5).

With the beginning of the growing season in the poplar plantation, transpiration (T_a) and interception evaporation (E_i) strongly increased, and relative extractable soil water (REW) decreased (Figure 6). Monthly evapotranspiration rates reached 150 mm during summer. In the wet year 2011, large amounts of precipitation temporarily replenished plant-available soil water in summer. In contrast, REW fell below the critical limit at 40% of its maximum value (Figure 6 b) in July and August 2012. During this period, T_a and E_i strongly collapsed, resulting in annual evapotranspiration of 2012 being reduced below 2011 by more than 100 mm (Table 6). In general, evapotranspiration and total runoff (D+R) were similar to the values obtained for deciduous beech forest that, however, had higher soil evaporation and lower interception evaporation (Table 6). On average, simulated annual transpiration was comparable to measured transpiration reported for a poplar SRF at a site with similar

soil properties but lower precipitation (Schmidt-Walter et al., 2014), and was lower than measured transpiration on a site with similar climate conditions (Petzold et al., 2011). Nonetheless, in both of these studies the sum of evapotranspiration (E) during the growing season (April-September) was lower than E of the Kaufering poplar SRF in that period (2011: 737 mm; 2012: 607 mm). On an annual timescale, SRF evapotranspiration in 2011 was 10% higher and in 2012 slightly lower (3%) then reference evaporation (ET_0, 2011: 775 mm, 2012: 754 mm) of a hypothetical, well-watered grass surface (Allen et al., 1998). Monthly evapotranspiration thereby regularly exceeded ET_0 during the growing season by 20-47%. Such evapotranspiration rates place our poplar plantation at the upper range of the SRF evapotranspiration spectrum (cf. Fischer et al., 2018, 2013), pointing to the magnitude of poplar water use that can be realized when water availability is high.

Precipitation in 2011 followed the characteristic mean annual course of the pre-alpine landscape, with the largest part of rain falling during the months of the growing season. In contrast, 2012 was characterized by a period of low rainfall in July and August. During this period, REW fell below the critical limit, and a transpiration deficit of 110 mm developed at the SRF. In terms of transpiration deficit (T_D), even higher drought stress was estimated for the evergreen spruce forest. However, the deciduous beech forest and the grassland vegetation were less affected by limited water availability in 2012 and showed higher transpiration rates than the poplar plantation (Table 6). At the SRF, a transpiration deficit of 42 mm surprisingly also accumulated during the wet growing season of 2011, when the grassland and beech forest simulations showed no indication of limited soil water availability. An explanation for relatively high transpiration deficits compared to the other vegetation types can be found in too high interception evaporation rates, caused by the very high canopy interception storage parameter (*cintrl*) estimated in the calibration (Figure 4). Simulated interception evaporation (E_i) of the poplar plantation amounted to 37% of precipitation during the months of the growing season. This is almost twice the proportion determined from field measurements in other poplar SRFs (10%-27% (Orság et al., 2013; Petzold et al., 2011; Schmidt-Walter et al., 2014), and suggests an overestimation of interception evaporation.

Simulated total evapotranspiration and relative extractable water can be regarded as accurate estimates, due to the high level of agreement between simulated and observed soil water storage. However, constraining the model solely on soil water storage probably resulted in biased partitioning of evapotranspiration towards interception losses. Overestimated interception losses decrease the actual amount of water infiltrating into the soil, thereby reducing water available for transpiration. Consequently, transpiration of the poplar plantation was probably underestimated and consequently, also the transpiration deficit was underestimated. To ultimately improve the prediction of individual water fluxes and transpiration deficits, the incorporation of additional observation datasets to further constrain the model on transpiration or net stand precipitation appears necessary.

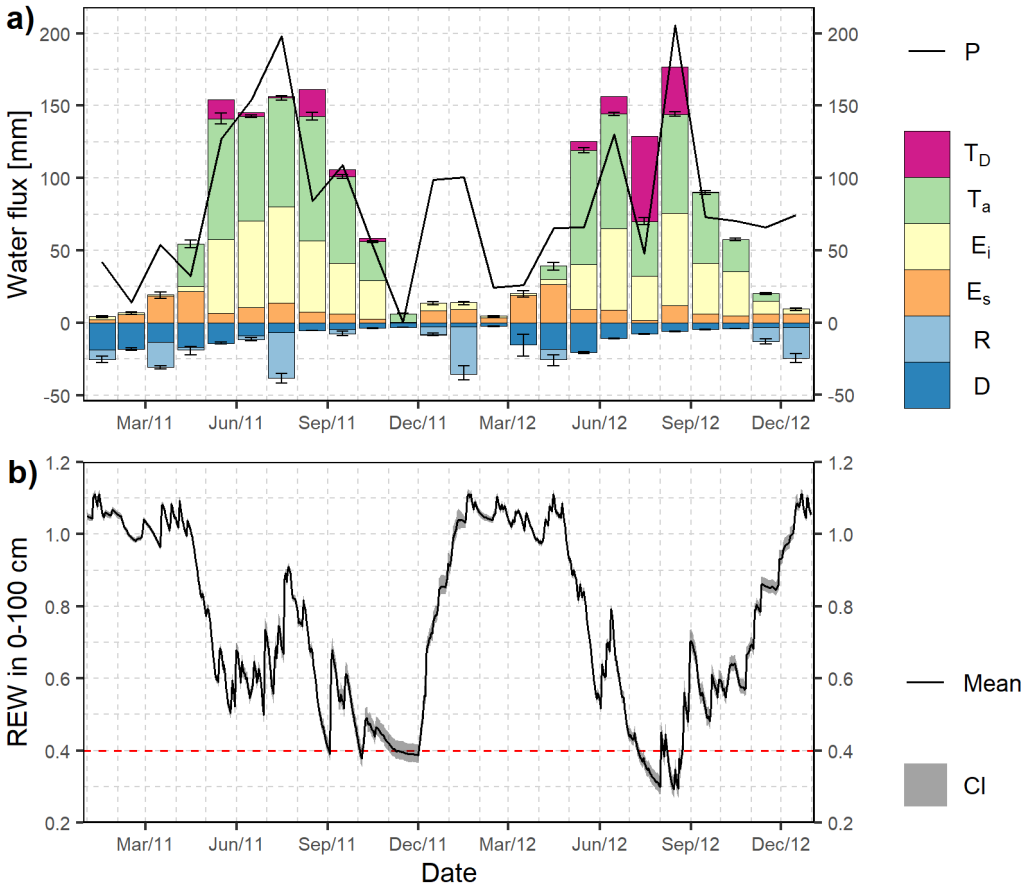

Figure 6 Final LWF-Brook90 model results for the poplar short rotation coppice. a) Mean (n= 1000) monthly water fluxes (T_a = transpiration, E_i = interception evaporation, E_s = soil evaporation, R = surface runoff, D = drainage), transpiration deficit (T_D), and precipitation (P), and b) relative extractable soil water storage (REW) in 0-100 cm soil depth. Error bars and uncertainty bounds denote the 95% confidence intervals of monthly evapotranspiration (T_a+E_i+E_s) and total runoff (D+R) (a), and REW (b).

Table 6: Predicted annual water fluxes (in mm y^{-1} ± std. dev.) for the Poplar SRF and the three vegetation covers (Table 1) at Kaufering (Germany).

	Year	Evapo-transpiration T_a+E_i+E_s	Transpiration T_a	Transpiration deficit T_D	Interception evaporation E_i	Soil evaporation E_s	Total runoff D+R
Poplar SRF	2011	844 ± 3.8	439 ± 5.8	42 ± 9.7	301 ± 2.9	104 ± 6.7	186 ± 2.7
	2012	733 ± 4.5	350 ± 4.1	110 ± 9.2	270 ± 2.3	113 ± 7.0	170 ± 5.2
Temp. deciduous forest	2011	813	405	1	268	140	198
	2012	779	381	27	261	136	157
Temp. evergreen forest	2011	1014	559	15	374	82	47
	2012	873	411	147	397	66	19
Temp. grassland	2011	704	438	2	113	153	278
	2012	667	416	7	116	136	275

4 Conclusions

The presented case study application illustrated how meaningful water flux and drought stress estimates of different vegetation types can be obtained, using existing parameter sets in LWFBrook90R. The results suggested that evergreen spruce forests are particularly vulnerable to cumulative-type droughts, due to incomplete soil water replenishment in winter. Cumulative droughts and extreme drought events severely affected forest functioning in Central Europe over 2018 and 2019 (Buras et al., 2019; Trotsiuk et al., 2020), and the intensity of such drought events is expected to increase in the coming decades (Teuling, 2018). SVAT and similar models in particular allow for the quantification of cumulative droughts that cannot be determined from bare soil and climatic data, such as the site water balance (Speich, 2019). In order to develop mitigation and adaptation strategies, we therefore need to be able to upscale these models for assessing the impacts of climate change on forest functions at a larger scale, for which the presented `LWFBrook90R` package provides convenient solutions.

Our case study further demonstrated the potential of state-of-the-art Bayesian calibrations and the ability of LWF-Brook90 to excellently capture the temporal variation of soil moisture. For a poplar short rotation forest (SRF), Bayesian calibration obtained a high degree of agreement between simulated and observed bulk soil water storage in the calibration (NSE = 0.96) and validation periods (NSE = 0.95). This enabled us to accurately estimate the plantation's annual water balance, with evapotranspiration rates of 844 mm (2011) and 733 mm (2012), that reflect the high water demand of these bioenergy systems. However, the results from the model calibration experiments also highlighted the increased demands placed on observational data by advanced inverse parameter estimation techniques. In our case, calibrating the model on observed soil water storage alone was probably associated with biased partitioning of evapotranspiration towards interception evaporation. The integration of additional datasets to further constrain the model on observed evaporation water fluxes, therefore, seems crucial to improve predictions of interception evaporation, transpiration and drought stress.

Large amounts of heterogeneous, harmonized high-quality observational ecosystem state and flux data of all kinds are increasingly becoming available through long-term ecosystem monitoring programs and data collections (Poyatos et al., 2016; Reyer et al., 2019), covering a wide range of climatic and soil conditions. Such data can well be used to calibrate the LWF-Brook90 model. However, a gap existed in combining a LWF-Brook90 with the various data streams. With our R package, we successfully filled this gap, and enabled a better integration of this particular model with data. Improved model data integration and the access to advanced statistical tools provides new opportunities for LWF-Brook90 to systematically assimilate observations into robust and reliable predictions of water fluxes and drought stress. Accordingly, these tools offer opportunities to improve

the predictive capacity of LWF-Brook90 in climate impact and risk assessments, e.g. by narrowing down prediction spans through combining heterogeneous datasets and additional field measurements to systematically constrain parameter uncertainties (LeBauer et al., 2013). Finally, the ability to run LWF-Brook90 directly from within R aids in scientific reporting and the reproducibility of simulation results through scripting of applications. The open source availability and platform-independent usability of `LWFBrook90R` will foster the widespread use of LWF-Brook90, and can advance our understanding of soil-vegetation-atmosphere interactions.

Acknowledgement

We thank Lothar Zimmermann and Stephan Raspe from the Bavarian State Institute of Forestry (LWF) for providing the LWF-Brook90 source code, as well as Klaus Hammel, Martin Kennel and Anthony Federer for agreeing to embed the code and publish the package under the GPL-3 license.

This work was supported by the projects "Forest productivity, carbon sequestration, climate change", funded by the Forest Climate Fund supported by the Federal Ministry of Food and Agriculture and the Federal Ministry for the Environment, Nature Conservation, Building and Nuclear Safety by decision of the German Bundestag (project no. 28WC4003), "Integrierter Klimaschutzplan Hessen 2025", funded by the Hessian Ministry of the Environment, Climate Protection, Agriculture and Consumer Protection, and "KLIP 11: Hydrologic and faunistic aspects and yield of a new established short rotation forest near Kaufering", funded by the Bavarian State Ministry of Food, Agriculture and Forestry. Additionally, the work was supported by the SwissForestLab research infrastructure.

References

Allen, C.D., Breshears, D.D., McDowell, N.G., 2015. On underestimation of global vulnerability to tree mortality and forest die-off from hotter drought in the Anthropocene. Ecosphere 6, art129. https://doi.org/10.1890/ES15-00203.1

Allen, C.D., Macalady, A.K., Chenchouni, H., Bachelet, D., McDowell, N., Vennetier, M., Kitzberger, T., Rigling, A., Breshears, D.D., Hogg, E.H. (Ted), Gonzalez, P., Fensham, R., Zhang, Z., Castro, J., Demidova, N., Lim, J.-H., Allard, G., Running, S.W., Semerci, A., Cobb, N., 2010. A global overview of drought and heat-induced tree mortality reveals emerging climate change risks for forests. For. Ecol. Manag., Adaptation of Forests and Forest Management to Changing Climate 259, 660–684. https://doi.org/10.1016/j.foreco.2009.09.001

Allen, R.G., Pereira, L.S., Raes, D., Smith, M., 1998. Crop evapotranspiration: guidelines for computing crop water requirements (No. 56), FAO Irrigation and drainage papers. FAO, Rome.

Arora, V., 2002. Modeling vegetation as a dynamic component in Soil-Vegetation-Atmosphere-Transfer schemes and hydrological models. Rev. Geophys. 40, 3-1-3–26. https://doi.org/10.1029/2001RG000103

Bagnara, M., Silveyra Gonzalez, R., Reifenberg, S., Steinkamp, J., Hickler, T., Werner, C., Dormann, C.F., Hartig, F., 2019. An R package facilitating sensitivity analysis, calibration and forward

simulations with the LPJ-GUESS dynamic vegetation model. Environ. Model. Softw. 111, 55–60. https://doi.org/10.1016/j.envsoft.2018.09.004
Baumgarten, M., Weis, W., Kühn, A., May, K., Matyssek, R., 2014. Forest transpiration—targeted through xylem sap flux assessment versus hydrological modeling. Eur. J. For. Res. 133, 677–690. https://doi.org/10.1007/s10342-014-0796-4
Beven, K., Binley, A., 1992. The future of distributed models: Model calibration and uncertainty prediction. Hydrol. Process. 6, 279–298. https://doi.org/10.1002/hyp.3360060305
Bouten, W., Jansson, P.-E., 1995. Water balance of the Solling spruce stand as simulated with various forest-soil-atmosphere models. Ecol. Model., Modelling Water, Carbon and Nutrient Cycles in Forests 83, 245–253. https://doi.org/10.1016/0304-3800(95)00102-2
Buras, A., Rammig, A., Zang, C.S., 2019. Quantifying impacts of the drought 2018 on European ecosystems in comparison to 2003. ArXiv190608605 Q-Bio Stat.
Clapp, R.B., Hornberger, G.M., 1978. Empirical Equations for Some Soil Hydraulic Properties. Water Resour. Res. 14, 601–604. https://doi.org/10.1029/WR014i004p00601
Conway, J., Eddelbuettel, D., Nishiyama, T., Prayaga, S.K., Tiffin, N., 2017. RPostgreSQL: R Interface to the "PostgreSQL" Database System.
Coron, L., Thirel, G., Delaigue, O., Perrin, C., Andréassian, V., 2017. The suite of lumped GR hydrological models in an R package. Environ. Model. Softw. 94, 166–171. https://doi.org/10.1016/j.envsoft.2017.05.002
De Cáceres, M., Martínez-Vilalta, J., Coll, L., Llorens, P., Casals, P., Poyatos, R., Pausas, J.G., Brotons, L., 2015. Coupling a water balance model with forest inventory data to predict drought stress: the role of forest structural changes vs. climate changes. Agric. For. Meteorol. 213, 77–90. https://doi.org/10.1016/j.agrformet.2015.06.012
De Cáceres, M., Martin-StPaul, N., Turco, M., Cabon, A., Granda, V., 2018. Estimating daily meteorological data and downscaling climate models over landscapes. Environ. Model. Softw. 108, 186–196. https://doi.org/10.1016/j.envsoft.2018.08.003
Federer, C.A., 2002. BROOK 90: A simulation model for evaporation, soil water, and streamflow. [WWW Document]. URL http://www.ecoshift.net/brook/brook90.htm (accessed 7.22.19).
Federer, C.A., Vörösmarty, C., Fekete, B., 2003. Sensitivity of Annual Evaporation to Soil and Root Properties in Two Models of Contrasting Complexity. J. Hydrometeorol. 4, 1276–1290. https://doi.org/10.1175/1525-7541(2003)004<1276:SOAETS>2.0.CO;2
Federer, C.A., Vörösmarty, C., Fekete, B., 1996. Intercomparison of methods for calculating potential evaporation in regional and global water balance models. Water Resour. Res. 32, 2315–2322. https://doi.org/10.1029/96WR00801
Fischer, M., Trnka, M., Kučera, J., Deckmyn, G., Orság, M., Sedlák, P., Žalud, Z., Ceulemans, R., 2013. Evapotranspiration of a high-density poplar stand in comparison with a reference grass cover in the Czech–Moravian Highlands. Agric. For. Meteorol. 181, 43–60. https://doi.org/10.1016/j.agrformet.2013.07.004
Fischer, M., Zenone, T., Trnka, M., Orság, M., Montagnani, L., Ward, E.J., Tripathi, A.M., Hlavinka, P., Seufert, G., Žalud, Z., King, J.S., Ceulemans, R., 2018. Water requirements of short rotation poplar coppice: Experimental and modelling analyses across Europe. Agric. For. Meteorol. 250–251, 343–360. https://doi.org/10.1016/j.agrformet.2017.12.079
Franks, S.W., Beven, K.J., Quinn, P.F., Wright, I., 1997. On the sensitivity of soil-vegetation-atmosphere transfer (SVAT) schemes: equifinality and the problem of robust calibration. Agric. For. Meteorol. 86, 63–75.
Frich, P., Alexander, L.V., Della-Marta, P., Gleason, B., Haylock, M., Tank, A.M.G.K., Peterson, T., 2002. Observed coherent changes in climatic extremes during the second half of the twentieth century. Clim. Res. 19, 193–212. https://doi.org/10.3354/cr019193
Fu, J., Gasche, R., Wang, N., Lu, H., Butterbach-Bahl, K., Kiese, R., 2017. Impacts of climate and management on water balance and nitrogen leaching from montane grassland soils of S-Germany. Environ. Pollut. Barking Essex 1987 229, 119–131. https://doi.org/10.1016/j.envpol.2017.05.071
Gale, M.R., Grigal, D.F., 1987. Vertical root distributions of northern tree species in relation to successional status. Can. J. For. Res. 17, 829–834. https://doi.org/10.1139/x87-131

673 Granier, A., Loustau, D., Breda, N., 2000. A generic model of forest canopy conductance dependent
674 on climate, soil water availability and leaf area index. Ann. For. Sci. 57, 755–765.
675 https://doi.org/10.1051/forest:2000158
676 Granier, A., Reichstein, M., Bréda, N., Janssens, I.A., Falge, E., Ciais, P., Grünwald, T., Aubinet, M.,
677 Berbigier, P., Bernhofer, C., Buchmann, N., Facini, O., Grassi, G., Heinesch, B., Ilvesniemi,
678 H., Keronen, P., Knohl, A., Köstner, B., Lagergren, F., Lindroth, A., Longdoz, B., Loustau,
679 D., Mateus, J., Montagnani, L., Nys, C., Moors, E., Papale, D., Peiffer, M., Pilegaard, K., Pita,
680 G., Pumpanen, J., Rambal, S., Rebmann, C., Rodrigues, A., Seufert, G., Tenhunen, J., Vesala,
681 T., Wang, Q., 2007. Evidence for soil water control on carbon and water dynamics in
682 European forests during the extremely dry year: 2003. Agric. For. Meteorol. 143, 123–145.
683 https://doi.org/10.1016/j.agrformet.2006.12.004
684 Groh, J., Puhlmann, H., 2013. Kalibrierung eines Bodenwasserhaushaltsmodells mit einer
685 kombinierten Zielfunktion für die Optimierung der Wasserretentionskurve [Calibration of a
686 soil-water balance model with a combined objective function for the optimization of the water
687 retention curve]. Hydrol. Wasserbewirtsch. 57, 152–163.
688 https://doi.org/10.5675/HyWa_2013,4_1
689 Hammel, K., Kennel, M., 2001. Charakterisierung und Analyse der Wasserverfügbarkeit und des
690 Wasserhaushalts von Waldstandorten in Bayern mit dem Simulationsmodell BROOK90,
691 Forstliche Forschungsberichte München.
692 Hanel, M., Kožín, R., Heřmanovský, M., Roub, R., 2017. An R package for assessment of statistical
693 downscaling methods for hydrological climate change impact studies. Environ. Model. Softw.
694 95, 22–28. https://doi.org/10.1016/j.envsoft.2017.03.036
695 Harlin, J., Kung, C.-S., 1992. Parameter uncertainty and simulation of design floods in Sweden. J.
696 Hydrol. 137, 209–230. https://doi.org/10.1016/0022-1694(92)90057-3
697 Hartig, F., Dyke, J., Hickler, T., Higgins, S.I., O'Hara, R.B., Scheiter, S., Huth, A., 2012. Connecting
698 dynamic vegetation models to data – an inverse perspective. J. Biogeogr. 39, 2240–2252.
699 https://doi.org/10.1111/j.1365-2699.2012.02745.x
700 Hartig, F., Minunno, F., Paul, S., 2019. BayesianTools: General-Purpose MCMC and SMC Samplers
701 and Tools for Bayesian Statistics.
702 Hornberger, G.M., Spear, R., 1981. An Approach to the Preliminary Analysis of Environmental
703 Systems. J Env. Manage U. S. 12:1.
704 Iturbide, M., Bedia, J., Herrera, S., Baño-Medina, J., Fernández, J., Frías, M.D., Manzanas, R., San-
705 Martín, D., Cimadevilla, E., Cofiño, A.S., Gutiérrez, J.M., 2019. The R-based climate4R open
706 framework for reproducible climate data access and post-processing. Environ. Model. Softw.
707 111, 42–54. https://doi.org/10.1016/j.envsoft.2018.09.009
708 Jackson, R.B., Canadell, J., Ehleringer, J.R., Mooney, H.A., Sala, O.E., Schulze, E.D., 1996. A global
709 analysis of root distributions for terrestrial biomes. Oecologia 108, 389–411.
710 https://doi.org/10.1007/BF00333714
711 Janssen, W., 2009. Definition des Vegetationsanfanges. Deutscher Wetterdienst, Abt.
712 Agrarmeteorologie, Offenbach.
713 Jansson, P.-E., Karlberg, L., 2004. Coupled heat and mass transfer model for soil-plant-atmosphere
714 systems. Royal Institute of Technolgy, Dept of Civil and Environmental Engineering
715 Stockholm, Stockholm.
716 LeBauer, D.S., Wang, D., Richter, K.T., Davidson, C.C., Dietze, M.C., 2013. Facilitating feedbacks
717 between field measurements and ecosystem models. Ecol. Monogr. 83, 133–154.
718 https://doi.org/10.1890/12-0137.1
719 Lebourgeois, F., Bréda, N., Ulrich, E., Granier, A., 2005. Climate-tree-growth relationships of
720 European beech (Fagus sylvatica L.) in the French Permanent Plot Network (RENECOFOR).
721 Trees 19, 385–401. https://doi.org/10.1007/s00468-004-0397-9
722 Lindner, M., Maroschek, M., Netherer, S., Kremer, A., Barbati, A., Garcia-Gonzalo, J., Seidl, R.,
723 Delzon, S., Corona, P., Kolström, M., Lexer, M.J., Marchetti, M., 2010. Climate change
724 impacts, adaptive capacity, and vulnerability of European forest ecosystems. For. Ecol.
725 Manag., Adaptation of Forests and Forest Management to Changing Climate 259, 698–709.
726 https://doi.org/10.1016/j.foreco.2009.09.023
727 Manrique-Alba, À., Ruiz-Yanetti, S., Moutahir, H., Novak, K., De Luis, M., Bellot, J., 2017. Soil
728 moisture and its role in growth-climate relationships across an aridity gradient in semiarid

Pinus halepensis forests. Sci. Total Environ. 574, 982–990. https://doi.org/10.1016/j.scitotenv.2016.09.123
Menzel, A., 1997. Phänologie von Waldbäumen unter sich ändernden Klimabedingungen - Auswertung der Beobachtungen in den Internationalen Phänologischen Gärten und Möglichkeiten der Modellierung von Phänodaten., Forstliche Forschungsberichte München.
Michelot, A., Bréda, N., Damesin, C., Dufrêne, E., 2012. Differing growth responses to climatic variations and soil water deficits of Fagus sylvatica, Quercus petraea and Pinus sylvestris in a temperate forest. For. Ecol. Manag. 265, 161–171. https://doi.org/10.1016/j.foreco.2011.10.024
Mualem, Y., 1976. A new model for predicting the hydraulic conductivity of unsaturated porous media. Water Resour. Res. 12, 513–522.
Netherer, S., Panassiti, B., Pennerstorfer, J., Matthews, B., 2019. Acute Drought Is an Important Driver of Bark Beetle Infestation in Austrian Norway Spruce Stands. Front. For. Glob. Change 2. https://doi.org/10.3389/ffgc.2019.00039
Nuske, R., 2017. vegperiod: Determine Thermal Vegetation Periods. https://doi.org/10.5281/zenodo.1466541
Orság, M., Fischer, M., Trnka, M., Pohanková, E., Poznikova, G., Žalud, Z., 2013. Role of interception and stem flow in water balance of short rotation poplar coppice.
Petzold, R., Schwärzel, K., Feger, K.-H., 2011. Transpiration of a hybrid poplar plantation in Saxony (Germany) in response to climate and soil conditions. Eur. J. For. Res. 130, 695–706. https://doi.org/10.1007/s10342-010-0459-z
Pianosi, F., Beven, K., Freer, J., Hall, J.W., Rougier, J., Stephenson, D.B., Wagener, T., 2016. Sensitivity analysis of environmental models: A systematic review with practical workflow. Environ. Model. Softw. 79, 214–232. https://doi.org/10.1016/j.envsoft.2016.02.008
Post, H., Vrugt, J.A., Fox, A., Vereecken, H., Franssen, H.-J.H., 2017. Estimation of Community Land Model parameters for an improved assessment of net carbon fluxes at European sites. J. Geophys. Res. Biogeosciences 122, 661–689. https://doi.org/10.1002/2015JG003297
Poyatos, R., Granda, V., Molowny-Horas, R., Mencuccini, M., Steppe, K., Martínez-Vilalta, J., 2016. SAPFLUXNET: towards a global database of sap flow measurements. Tree Physiol. 36, 1449–1455. https://doi.org/10.1093/treephys/tpw110
Puhlmann, H., von Wilpert, K., 2012. Pedotransfer functions for water retention and unsaturated hydraulic conductivity of forest soils. J. Plant Nutr. Soil Sci. 175, 221–235. https://doi.org/10.1002/jpln.201100139
Pujol, G., Iooss, B., Janon, A., Boumhaout, K., Da Veiga, S., Fruth, J., Gilquin, L., Guillaume, J., Le Gratiet, L., Lemaitre, P., others, 2016. Sensitivity: global sensitivity analysis of model outputs. R Package Version 1.
Pullens, J.W.M., Bagnara, M., Silveyra González, R., Gianelle, D., Sottocornola, M., Heijmans, M.M.P.D., Kiely, G., Hartig, F., 2017. The NUCOMBog R package for simulating vegetation, water, carbon and nitrogen dynamics in peatlands. Ecol. Inform. 40, 35–39. https://doi.org/10.1016/j.ecoinf.2017.05.001
R Core Team, 2019. R: A Language and Environment for Statistical Computing. R Foundation for Statistical Computing, Vienna, Austria.
Raj, R., Tol, C. van der, Hamm, N.A.S., Stein, A., 2018. Bayesian integration of flux tower data into a process-based simulator for quantifying uncertainty in simulated output. Geosci. Model Dev. 11, 83–101. https://doi.org/10.5194/gmd-11-83-2018
Reyer, C.P.O., Silveyra Gonzalez, R., Dolos, K., Hartig, F., Hauf, Y., Noack, M., Lasch-Born, P., Rötzer, T., Pretzsch, H., Mesenburg, H., Fleck, S., Wagner, M., Bolte, A., Sanders, T.G.M., Kolari, P., Mäkelä, A., Vesala, T., Mammarella, I., Pumpanen, J., Collalti, A., Trotta, C., Matteucci, G., D'Andrea, E., Foltýnová, L., Krejza, J., Ibrom, A., Pilegaard, K., Loustau, D., Bonnefond, J.-M., Berbigier, P., Picart, D., Lafont, S., Dietze, M., Cameron, D., Vieno, M., Tian, H., Palacios-Orueta, A., Cicuendez, V., Recuero, L., Wiese, K., Büchner, M., Lange, S., Volkholz, J., Kim, H., Weedon, G.P., Sheffield, J., Vega del Valle, I., Suckow, F., Horemans, J.A., Martel, S., Bohn, F., Steinkamp, J., Chikalanov, A., Mahnken, M., Gutsch, M., Frieler, K., 2019. The PROFOUND database for evaluating vegetation models and simulating climate impacts on forests. Earth Syst. Sci. Data Discuss. 1–47. https://doi.org/10.5194/essd-2019-220

Richter, D., 1995. Ergebnisse methodischer Untersuchungen zur Korrektur des systematischen Messfehlers des Hellmann-Niederschlagsmessers. (No. 194), Berichte des Deutschen Wetterdienstes. Deutscher Wetterdienst, Offenbach.

Ruffault, J., Martin-StPaul, N.K., Duffet, C., Goge, F., Mouillot, F., 2014. Projecting future drought in Mediterranean forests: bias correction of climate models matters! Theor. Appl. Climatol. 117, 113–122. https://doi.org/10.1007/s00704-013-0992-z

Ruffault, J., Martin-StPaul, N.K., Rambal, S., Mouillot, F., 2013. Differential regional responses in drought length, intensity and timing to recent climate changes in a Mediterranean forested ecosystem. Clim. Change 117, 103–117. https://doi.org/10.1007/s10584-012-0559-5

Saltelli, A., Ratto, M., Andres, T., Campolongo, F., Cariboni, J., Gatelli, D., Saisana, M., Tarantola, S., 2008. Global Sensitivity Analysis: The Primer. John Wiley & Sons, Ltd, Chichester, England.

Schmidt-Walter, P., Ahrends, B., Mette, T., Puhlmann, H., Meesenburg, H., 2019. NFIWADS: the water budget, soil moisture, and drought stress indicator database for the German National Forest Inventory (NFI). Ann. For. Sci. 76, 39. https://doi.org/10.1007/s13595-019-0822-2

Schmidt-Walter, P., Richter, F., Herbst, M., Schuldt, B., Lamersdorf, N.P., 2014. Transpiration and water use strategies of a young and a full-grown short rotation coppice differing in canopy cover and leaf area. Agric. For. Meteorol. 195–196, 165–178. https://doi.org/10.1016/j.agrformet.2014.05.006

Schwärzel, K., Feger, K.-H., Häntzschel, J., Menzer, A., Spank, U., Clausnitzer, F., Köstner, B., Bernhofer, C., 2009. A novel approach in model-based mapping of soil water conditions at forest sites. For. Ecol. Manag., Forest Soil Science: Celebrating 50 Years of Research on Properties, Processes and Management of Forest Soils Forest Soil Science: Celebrating 50 Years of Research on Properties, Processes and Management of Forest Soils Forest Soil Science: Celebrating 50 Years of Research on Properties, Processes and Management of Forest Soils Forest Soil Science: Celebrating 50 Years of Research on Properties, Processes and Management of Forest Soils Selected and Edited Papers from the Eleventh North American Forest Soils Conference held June 22-26, 2008 in Blacksburg, Virginia, USA 258, 2163–2174. https://doi.org/10.1016/j.foreco.2009.03.033

Seidl, R., Baier, P., Rammer, W., Schopf, A., Lexer, M.J., 2007. Modelling tree mortality by bark beetle infestation in Norway spruce forests. Ecol. Model. 206, 383–399. https://doi.org/10.1016/j.ecolmodel.2007.04.002

Seidl, R., Thom, D., Kautz, M., Martin-Benito, D., Peltoniemi, M., Vacchiano, G., Wild, J., Ascoli, D., Petr, M., Honkaniemi, J., Lexer, M.J., Trotsiuk, V., Mairota, P., Svoboda, M., Fabrika, M., Nagel, T.A., Reyer, C.P.O., 2017. Forest disturbances under climate change. Nat. Clim. Change 7, 395–402. https://doi.org/10.1038/nclimate3303

Slater, L.J., Thirel, G., Harrigan, S., Delaigue, O., Hurley, A., Khouakhi, A., Prosdocimi, I., Vitolo, C., Smith, K., 2019. Using R in hydrology: a review of recent developments and future directions. Hydrol. Earth Syst. Sci. 23, 2939–2963. https://doi.org/10.5194/hess-23-2939-2019

Song, X., Bryan, B.A., Almeida, A.C., Paul, K.I., Zhao, G., Ren, Y., 2013. Time-dependent sensitivity of a process-based ecological model. Ecol. Model. 265, 114–123. https://doi.org/10.1016/j.ecolmodel.2013.06.013

Song, X., Zhang, J., Zhan, C., Xuan, Y., Ye, M., Xu, C., 2015. Global sensitivity analysis in hydrological modeling: Review of concepts, methods, theoretical framework, and applications. J. Hydrol. 523, 739–757. https://doi.org/10.1016/j.jhydrol.2015.02.013

Speich, M.J.R., 2019. Quantifying and modeling water availability in temperate forests: a review of drought and aridity indices. IForest - Biogeosciences For. 12, 1. https://doi.org/10.3832/ifor2934-011

Speich, M.J.R., Zappa, M., Scherstjanoi, M., Lischke, H., 2020. FORests and HYdrology under Climate Change in Switzerland v1.0: a spatially distributed model combining hydrology and forest dynamics. Geosci. Model Dev. 13, 537–564. https://doi.org/10.5194/gmd-13-537-2020

ter Braak, C.J.F., Vrugt, J.A., 2008. Differential Evolution Markov Chain with snooker updater and fewer chains. Stat. Comput. 18, 435–446. https://doi.org/10.1007/s11222-008-9104-9

Teuling, A.J., 2018. A hot future for European droughts. Nat. Clim. Change 8, 364–365. https://doi.org/10.1038/s41558-018-0154-5

Thiele, J.C., Nuske, R.S., Ahrends, B., Panferov, O., Albert, M., Staupendahl, K., Junghans, U., Jansen, M., Saborowski, J., 2017. Climate change impact assessment—A simulation experiment with Norway spruce for a forest district in Central Europe. Ecol. Model. 346, 30–47. https://doi.org/10.1016/j.ecolmodel.2016.11.013

Trotsiuk, V., Hartig, F., Cailleret, M., Babst, F., Forrester, D.I., Baltensweiler, A., Buchmann, N., Bugmann, H., Gessler, A., Gharun, M., Minunno, F., Rigling, A., Rohner, B., Stillhard, J., Thürig, E., Waldner, P., Ferretti, M., Eugster, W., Schaub, M., 2020. Assessing the response of forest productivity to climate extremes in Switzerland using model–data fusion. Glob. Change Biol. 26, 2463–2476. https://doi.org/10.1111/gcb.15011

van der Salm, C., Reinds, G.J., de Vries, W., 2007. Water balances in intensively monitored forest ecosystems in Europe. Environ. Pollut. 148, 201–212. https://doi.org/10.1016/j.envpol.2006.10.043

van Genuchten, T., 1980. A Closed-form Equation for Predicting the Hydraulic Conductivity of Unsaturated Soils. Soil Sci. Soc. Am. J. 44, 892–898. https://doi.org/10.2136/sssaj1980.03615995004400050002x

van Oijen, M., 2017. Bayesian Methods for Quantifying and Reducing Uncertainty and Error in Forest Models. Curr. For. Rep. 3, 269–280. https://doi.org/10.1007/s40725-017-0069-9

von Wilpert, K., 1991. Intraannual variation of radial tracheid diameters as monitor of site specific water stress. Dendrochronologia 9, 95–113.

von Wilpert, K., 1990. Die Jahrringstruktur von Fichten in Abhängigkeit vom Bodenwasserhaushalt auf Pseudogley und Parabraunerde: Ein Methodenkonzept zur Erfassung standortsspezifischer Wasserstreßdispostion, Freiburger Bodenkundliche Abhandlungen. Freiburg.

Weis, W., Hertel, C., Wagner, A., Raspe, S., 2012. Verbesserung der Wasserhaushaltsmodellierung mit Daten des forstlichen Umweltmonitorings im Projekt FUTMON (LIFE+) (No. ST241). Landesanstalt für für Wald und Forstwirtschaft (LWF), Freising.

Wu, Y., Liu, S., 2012. Automating calibration, sensitivity and uncertainty analysis of complex models using the R package Flexible Modeling Environment (FME): SWAT as an example. Environ. Model. Softw. 31, 99–109. https://doi.org/10.1016/j.envsoft.2011.11.013